Lee *et al. Cancer Cell International* (2025) 25:444
https://doi.org/10.1186/s12935-025-04082-5

Cancer Cell International

RESEARCH Open Access

Restoration of BAP1 activity via base editing suppresses anchorage-independent survival in kidney cancer

Daye Lee[1], Boram Lee[1], Jiyeon Lee[1] and Jongbum Kwon[1*]

Abstract

BAP1, a deubiquitinase with a ubiquitin C-terminal hydrolase domain, functions as a tumor suppressor involved in diverse cellular processes, including DNA repair, genome stability, and apoptosis. Inactivating mutations in BAP1—particularly missense and deletion variants—are recurrent across multiple cancers, with a high prevalence in clear cell renal cell carcinoma (ccRCC), mesothelioma, and uveal melanoma. Among these, the Glu31Lys mutation in ccRCC impairs BAP1's enzymatic activity, protein stability, and DNA repair functions. Here, we investigated the physiological impact of this recurrent mutation using isogenic KMRC-20 ccRCC cell clones in which the Glu31Lys substitution was precisely corrected to wild-type glutamate via CRISPR-Cas9–mediated adenine base editing. BAP1 reactivation restored anchorage-dependent growth in KMRC-20 cells—a hallmark of non-transformed epithelial cells—and increased apoptosis under non-adherent conditions, indicating reinstated sensitivity to anoikis. Mechanistically, this phenotypic switch was accompanied by post-transcriptional downregulation of N-cadherin and β-catenin under anchorage-free conditions, implicating BAP1 in the regulation of adhesion- and Wnt-related survival pathways. Furthermore, transcriptomic profiling revealed broad gene expression changes upon BAP1 restoration, suggesting that these combined alterations contribute to the re-establishment of anchorage-dependent growth in KMRC-20 cells. These findings uncover a previously unrecognized role for BAP1 in suppressing anchorage-independent survival, providing new insights into BAP1-driven tumorigenesis and underscoring the therapeutic potential of precise gene editing to restore tumor suppressor function in ccRCC.

Keywords BAP1 tumor suppressor, Kidney cancer, Anchorage-dependent growth, Apoptosis, CRISPR-Cas9–mediated adenine base editing

*Correspondence:
Jongbum Kwon
jongkwon@ewha.ac.kr
[1]Department of Life Science, Ewha Womans University, 52 Ewhayeodae-gil, Seodaemun-gu, Seoul 03760, Korea

© The Author(s) 2025. **Open Access** This article is licensed under a Creative Commons Attribution-NonCommercial-NoDerivatives 4.0 International License, which permits any non-commercial use, sharing, distribution and reproduction in any medium or format, as long as you give appropriate credit to the original author(s) and the source, provide a link to the Creative Commons licence, and indicate if you modified the licensed material. You do not have permission under this licence to share adapted material derived from this article or parts of it. The images or other third party material in this article are included in the article's Creative Commons licence, unless indicated otherwise in a credit line to the material. If material is not included in the article's Creative Commons licence and your intended use is not permitted by statutory regulation or exceeds the permitted use, you will need to obtain permission directly from the copyright holder. To view a copy of this licence, visit http://creativecommons.org/licenses/by-nc-nd/4.0/.

Introduction

BRCA1-associated protein-1 (BAP1) is a deubiquitinase (DUB) containing a ubiquitin C-terminal hydrolase (UCH) domain and functions as a tumor suppressor [1, 2]. It is involved in a wide range of chromatin-associated processes, including transcription, DNA replication, DNA damage repair, and the maintenance of genome stability [3–9]. In addition, BAP1 plays key roles in various physiological processes such as cell proliferation, differentiation, development, metabolism, and cell death [10–18]. BAP1 operates in both the nucleus and the cytoplasm, and its subcellular localization is tightly regulated. Specifically, BAP1 undergoes monoubiquitination at multiple sites within its nuclear localization signal (NLS), resulting in its retention in the cytoplasm. To counteract this, BAP1 can autodeubiquitinate its NLS, enabling its translocation into the nucleus where it can carry out its nuclear functions [19]. One of BAP1's major substrates is histone H2A monoubiquitinated at lysine 119 (H2A-Ub), a critical epigenetic mark that regulates transcription, replication and DNA repair [20].

Inherited mutations in the BAP1 gene are closely linked to increased susceptibility to several cancers, with a particularly high incidence in clear cell renal cell carcinoma (ccRCC), mesothelioma, and uveal melanoma [21–23]. These germline alterations markedly elevate cancer risk in affected individuals and are the defining feature of BAP1 cancer syndrome. This hereditary tumor predisposition syndrome is characterized by the occurrence of one or more malignancies and exhibits an exceptionally high penetrance, nearing complete expression among mutation carriers [24, 25]. In addition to germline variants, somatic mutations in BAP1 are frequently detected in tumors arising in these patients. While the majority of cancer-associated BAP1 mutations consist of missense point mutations or truncating deletions, the precise functional consequences and molecular mechanisms underlying their oncogenic potential remain poorly understood [24, 26].

Recent studies have uncovered a key role for BAP1 in the nucleotide excision repair (NER) pathway responsible for resolving UV-induced DNA damage [27]. In this context, we identified glutamate 31 (Glu31)—a residue frequently mutated in cancers such as ccRCC—as a critical regulator of this repair process. Following UV irradiation, BAP1 is recruited to chromatin and accumulates at DNA damage sites, where it promotes repair in a manner dependent on its catalytic activity. This recruitment is facilitated by interactions with PARP1 and H2A-Ub, both of which are enhanced upon UV exposure. Importantly, UV-induced poly(ADP-ribosyl)ation (PARylation) of BAP1 by PARP1 occurs at multiple sites, including Glu31. Substitution of Glu31 with alanine, a residue that cannot be PARylated, leads to reduced BAP1 protein stability and impaired DNA repair. Even when expressed at normal levels, this mutant form of BAP1 is unable to rescue the repair defect, indicating that Glu31 plays an essential role in functions beyond protein stabilization [27]. Subsequent investigation revealed that Glu31 is crucial for BAP1's DUB activity, enhancing its affinity for ubiquitin through salt bridge formation with Arg72. Moreover, PARylation inhibits BAP1 activity, providing a dynamic mode of enzymatic regulation.

Further evidence supporting the functional significance of Glu31 comes from experiments in KMRC-20 cells, a kidney cancer cell line bearing a Glu31Lys mutation as the sole alteration in the BAP1 gene. Re-expression of wild-type BAP1 in these cells significantly reduced cell viability, while the Glu31Ala mutant did not, even when comparably expressed. A similar trend was observed in UMRC-6, another kidney cancer cell line lacking endogenous BAP1 expression: while introduction of wild-type BAP1 significantly decreased cell viability, the Glu31Ala mutant again had no impact, despite being expressed at normal levels [27]. These findings suggest that loss of Glu31 function may contribute to the tumorigenic potential of BAP1 mutations in kidney cancer.

In the present study, we sought to determine whether restoration of Glu31 in KMRC-20 cells could suppress tumorigenic features. Using CRISPR-Cas9-driven adenine base editing (ABE), we reverted the Lys31 mutation to wild-type Glu31, generating isogenic cell lines. Remarkably, these revertant cells displayed anchorage-dependent growth, a hallmark of non-transformed, normal cells. This phenotype was linked to increased apoptosis following loss of cell adhesion in culture, suggesting restored sensitivity to anoikis. Additionally, our data indicate that this anchorage dependence may be mediated through the N-cadherin and Wnt/β-catenin signaling pathways. These findings highlight the importance of the catalytically essential residue Glu31 in supporting anchorage-dependent growth and suggest a potential mechanism through which BAP1 mutations may contribute to tumorigenesis.

Results

Correction of the Glu31 mutation in KMRC-20 cells via base editing

To assess the functional impact of the Glu31 mutation in the BAP1 gene on the tumorigenic properties of KMRC-20 cells, we employed CRISPR/Cas9-mediated adenine base editing to revert this alteration [28, 29]. Specifically, we used the ABE7.10max base editor in combination with the VRQR Cas9 variant [30], which recognizes an AGAG protospacer adjacent motif (PAM) sequence (corresponding to the degenerate NGAG PAM in the *BAP1* locus) (Fig. 1A). A lentiviral construct was engineered to co-express this base editor along with a guide

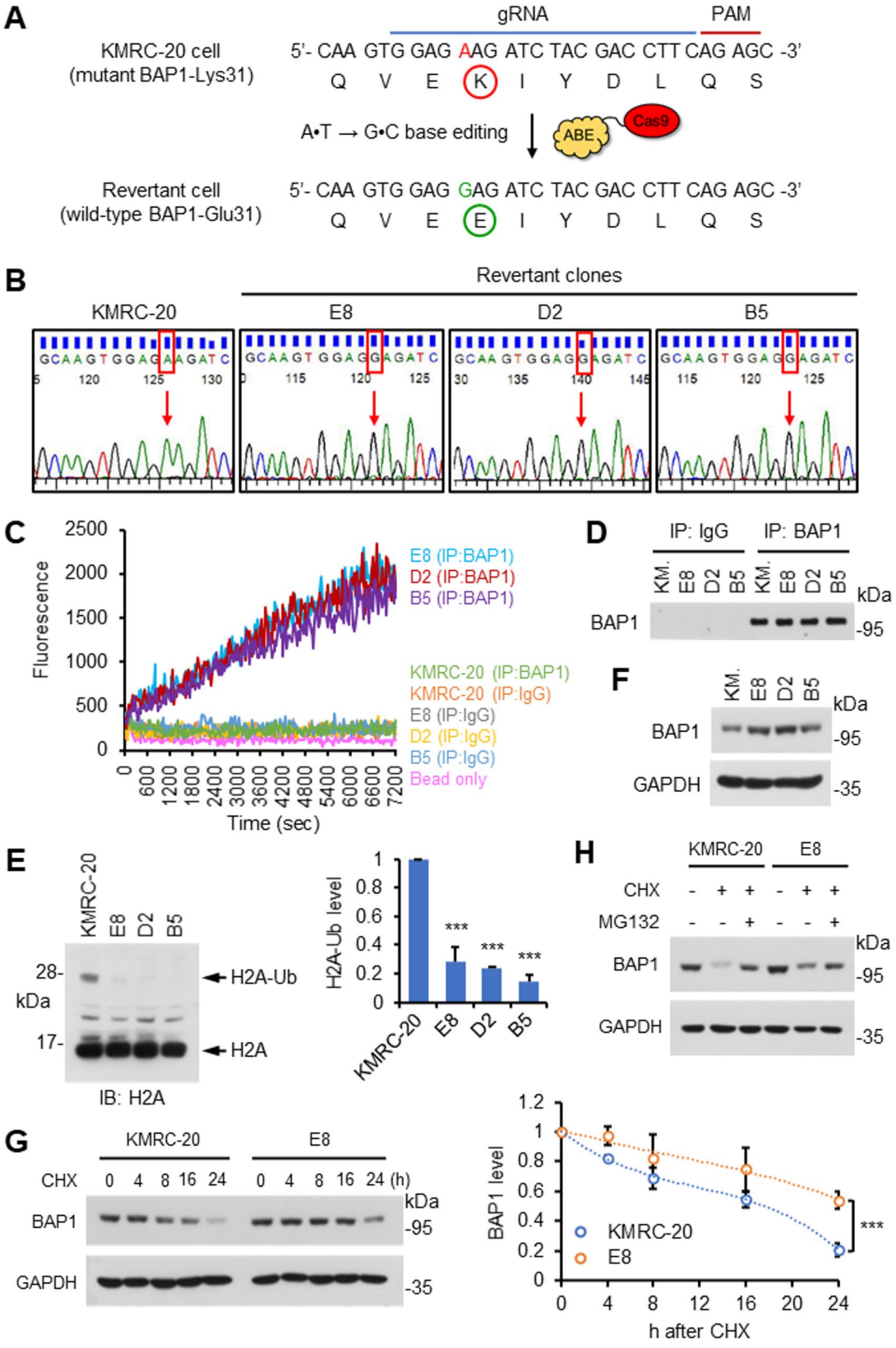


Fig. 1 (See legend on next page.)

(See figure on previous page.)

Fig. 1 Generation of isogenic KMRC-20 cells with restored BAP1 activity via adenine base editing (**A**) Schematic of A•T → G•C base editing strategy to correct the Glu31Lys (AAG) mutation to wild-type glutamate (GAG) in KMRC-20 cells. The adenine to be edited (red) is converted to guanine (green). The gRNA and PAM sequences are indicated by blue and red lines, respectively. The ABE7.10max-VRQR variant, recognizing AGAG as the PAM, was engineered to target the BAP1 gene and edits the adenine at the fifth position from the 5′ end with highest efficiency. (**B**) Sequencing of genomic DNA from parental and three independent revertant KMRC-20 clones showing precise correction of the Glu31Lys mutation. (**C**, **D**) Ub-AMC deubiquitinase (DUB) assay using BAP1 immune complexes. Lysates from parental and revertant cells were immunoprecipitated with anti-BAP1 or control IgG; one fraction was analyzed for DUB activity (C), and the other for BAP1 protein levels by immunoblotting (D). Representative of three independent experiments. Fluorescence values (reflecting AMC release) are presented as relative fluorescence units (RFU). (**E**) Immunoblot analysis of H2A ubiquitination (H2A-Ub) in parental and revertant cells. Quantification is shown to the right; H2A-Ub levels were normalized to total H2A, with parental KMRC-20 set to 1 ($n = 3$; mean ± s.d.). (**F**) Steady-state BAP1 protein levels assessed by immunoblotting in parental and revertant clones. (**G**) Cycloheximide (CHX) chase assay showing BAP1 protein decay. KMRC-20 and E8 cells were treated with CHX for up to 24 h; BAP1 levels were normalized to GAPDH and expressed relative to time 0 ($n = 3$; mean ± s.d.). (**H**) BAP1 stability is regulated via the ubiquitin–proteasome pathway. Cells were treated with CHX for 24 h in the presence or absence of MG132, followed by immunoblot analysis of BAP1

RNA (gRNA) designed to target the AAG codon (encoding Lys31) and convert it to GAG (encoding Glu31) (Fig. 1A). Following lentiviral infection and puromycin selection under limiting dilution, we successfully isolated three independent single-cell clones—designated E8, D2, and B5—in which the first nucleotide of the AAG codon had been precisely edited to guanine (Fig. 1B). Chromosome analysis confirmed that KMRC-20 cells are triploid, carrying three copies of each chromosome (Fig. S1A). Sequencing of genomic DNA from the edited clones revealed a single, distinct guanine peak at the first base of the codon for Glu31 (Fig. 1B), indicating that all three alleles of the BAP1 gene had been successfully edited. In addition, sequence analysis of the top three predicted off-target sites showed no detectable base substitutions in the edited clones (Fig. S1B), confirming the specificity of the editing strategy.

We next examined whether the revertant KMRC-20 clones restored BAP1 enzymatic activity and protein stability. To assess DUB activity, BAP1 was immunoprecipitated from the revertant cells, and its activity was measured using Ub-AMC, a fluorogenic ubiquitin substrate. As expected, immunoprecipitated BAP1 from parental KMRC-20 cells exhibited no detectable DUB activity. In contrast, BAP1 isolated from all three revertant clones displayed robust DUB activity, while IgG control immunoprecipitates showed none, confirming that enzymatic function was successfully restored (Fig. 1C, D). Consistent with this, the cellar levels of H2A-Ub—a direct substrate of BAP1—were significantly reduced in the revertant clones compared to KMRC-20 cells (Fig. 1E). In addition, steady-state BAP1 protein levels were elevated in the revertant cells (Fig. 1F), suggesting improved protein stability. Cycloheximide chase assays using the E8 clone as a representative example confirmed this, revealing a prolonged BAP1 half-life relative to parental cells (Fig. 1G). Similar to KMRC-20 cells, treatment with the proteasome inhibitor MG132 restored BAP1 protein levels that had been reduced by cycloheximide (Fig. 1H), indicating that BAP1 degradation in the revertant clone remains proteasome-dependent. Taken together, these results demonstrate that the Glu31-to-Lys mutation produces a catalytically inactive and unstable form of BAP1, and that base editing successfully reestablished wild-type BAP1 function and stability in the isogenic revertant lines.

Correction of the Glu31 mutation has minimal impact on KMRC-20 cell growth and proliferation

Given that re-expression of wild-type BAP1—but not the Glu31-to-Lys mutant—reduces the viability of KMRC-20 cells [27], we next sought to determine whether correction of the endogenous Glu31 mutation would similarly affect cell viability and proliferation in the revertant clones. Microscopic examination revealed that all three revertant clones exhibited morphologies indistinguishable from the parental KMRC-20 cells (Fig. 2A). Short-term viability assays showed that the revertant clones displayed no significant changes or only modest increases in cell viability and growth rates compared to KMRC-20 (Fig. 2B). In line with these findings, cell cycle analysis revealed comparable profiles between the revertant and parental cells, each displaying the typical biphasic DNA content peaks associated with G1 and G2/M phases (Fig. 2C). Additionally, the percentage of sub-G1 cells, an indicator of cell death, was similar between the revertant and parental lines (Fig. 2C), suggesting no increase in apoptosis following correction of the Glu31 mutation. Interestingly, results from a long-term clonogenic assay indicated some variability among clones. Clones E8 and D2 exhibited a notable increase in colony-forming ability, whereas B5 showed a slight reduction compared to KMRC-20 (Fig. 2D). Despite these differences, none of the revertant clones demonstrated a consistent or substantial impairment in proliferation, cell cycle progression, or viability. These findings suggest that, contrary to our initial expectation, restoring the Glu31 residue in BAP1 does not significantly impair cell growth or survival under standard culture conditions. The previously observed reduction in viability upon exogenous wild-type BAP1 expression may reflect non-physiological effects of overexpression, rather than an inherent consequence of restoring BAP1 function.

Correction of the Glu31 mutation restores anchorage-dependent growth in KMRC-20 cells

We next investigated whether correction of the Glu31 mutation impacts the anchorage-independent growth characteristic of KMRC-20 cells. In soft agar assays, all three revertant clones showed a marked reduction in colony formation compared to the parental cells, with clone B5 displaying virtually no colonies (Fig. 3A, B). These findings indicate that restoration of BAP1 activity renders KMRC-20 cells anchorage-dependent, a key feature of non-tumorigenic cells.

While characterizing the initial revertant clones, we observed that some lost anchorage-dependent growth. Genomic sequencing of these clones revealed that this phenotype was associated with unintended bystander base edits affecting adenine nucleotides within the Glu31 codon as well as the adjacent Glu30 codon (Fig. S2A). These alterations were likely caused by persistent ABE-Cas9 activity from stably integrated lentiviral vectors (Fig. S2B). To avoid this, we used transient transfection to deliver the ABE-Cas9 construct, limiting the duration of base editor expression. Using a similar single-cell cloning and screening strategy, we established a new set of revertant KMRC-20 clones, designated 1–1, 1–3, and 1–34. Sequencing confirmed successful correction of the Glu31 codon without any detectable changes at the top three predicted off-target sites, consistent with the earlier clones (Fig. S2C, D).

As with the original clones, we confirmed restored BAP1 activity through Ub-AMC DUB assays (Fig. S3A), reduced H2A-Ub levels (Fig. S3B), and elevated BAP1 protein levels (Fig. S3C). Furthermore, clone 1–34 was able to rescue the UV-induced DNA repair defect observed in KMRC-20 cells (Fig. S3D), confirming restoration of not only BAP1's catalytic activity but also its functional role in the DNA damage response. The new clones also resembled the parental cells in morphology (Fig. S4A), short-term viability (Fig. S4B), and cell cycle profile (Fig. S4C). As before, long-term clonogenic potential varied: clone 1–1 showed a modest increase, while 1–3 and 1–34 showed decreased colony formation (Fig. S4D). Importantly, these clones no longer expressed ABE-Cas9 after editing, and no bystander edits were observed over extended culture (Fig. S2B).

We next tested whether these new clones restored anchorage-dependent growth using soft agar assays. Notably, clone 1–1 showed a marked reduction in colony formation under anchorage-independent conditions relative to parental KMRC-20 cells, while clones 1–3 and 1–34 formed virtually no colonies (Fig. 3C, D). Together, using two independent sets of three revertant clones, each generated by distinct ABE-Cas9 delivery methods, we demonstrate that correction of the Glu31 mutation restores anchorage-dependent growth in KMRC-20 cells—strongly supporting a role for BAP1 in suppressing anchorage-independent, tumorigenic behavior. These new revertant clones were used in the following studies to investigate the mechanisms behind restored anchorage-dependent growth.

Correction of the Glu31 mutation induces apoptosis upon anchorage loss in KMRC-20 cells

To investigate the mechanisms underlying the restored anchorage-dependent growth in the revertant KMRC-20 clones, we examined whether increased cell death upon detachment could account for the observed phenotype. Cells were cultured in ultra-low attachment (ULA) dishes, which mimic anchorage-independent conditions and simulate anoikis, a form of apoptosis triggered by loss of adhesion [31, 32]. Annexin V/PI staining revealed significantly increased cell death in all three revertant clones compared to parental KMRC-20 cells under ULA conditions (Fig. 4A). This increase was largely attributed to apoptosis, with necrosis playing a minimal role. Importantly, no difference in cell death was observed between revertant and parental cells when cultured under normal adherent conditions (Fig. 4A). To further confirm apoptosis, we assessed cleavage of PARP1, a hallmark of apoptotic signaling [33]. Under ULA conditions, PARP1 cleavage was markedly elevated in all three revertant clones relative to the parental cells, whereas levels remained comparable under adherent conditions (Fig. 4B). These results indicate that the inability of the revertant KMRC-20 cells to proliferate without adhesion, as seen in the soft agar assay, is due to increased apoptosis triggered by anchorage loss, consistent with reactivation of a tumor-suppressive anoikis response.

N-cadherin and β-catenin are downregulated in revertant KMRC-20 cells following anchorage loss

To investigate molecular pathways associated with the restored anchorage-dependent growth in the revertant KMRC-20 cells, we focused on N-cadherin, β-catenin, and vimentin—key proteins involved in cell adhesion, pro-survival signaling, and epithelial-to-mesenchymal transition (EMT). N-cadherin is a central mediator of cell–cell adhesion and is frequently upregulated in cancer cells to promote survival under anchorage-independent conditions, contributing to anoikis resistance [34, 35]. β-catenin functions downstream of N-cadherin and the Wnt pathway, supporting both cell adhesion and transcriptional activation of genes involved in proliferation and metastasis [36, 37]. Vimentin, a canonical EMT marker, was included as a control to determine whether the observed phenotype involved a broad EMT reversal or a more selective change in adhesion-related signaling [34, 38].

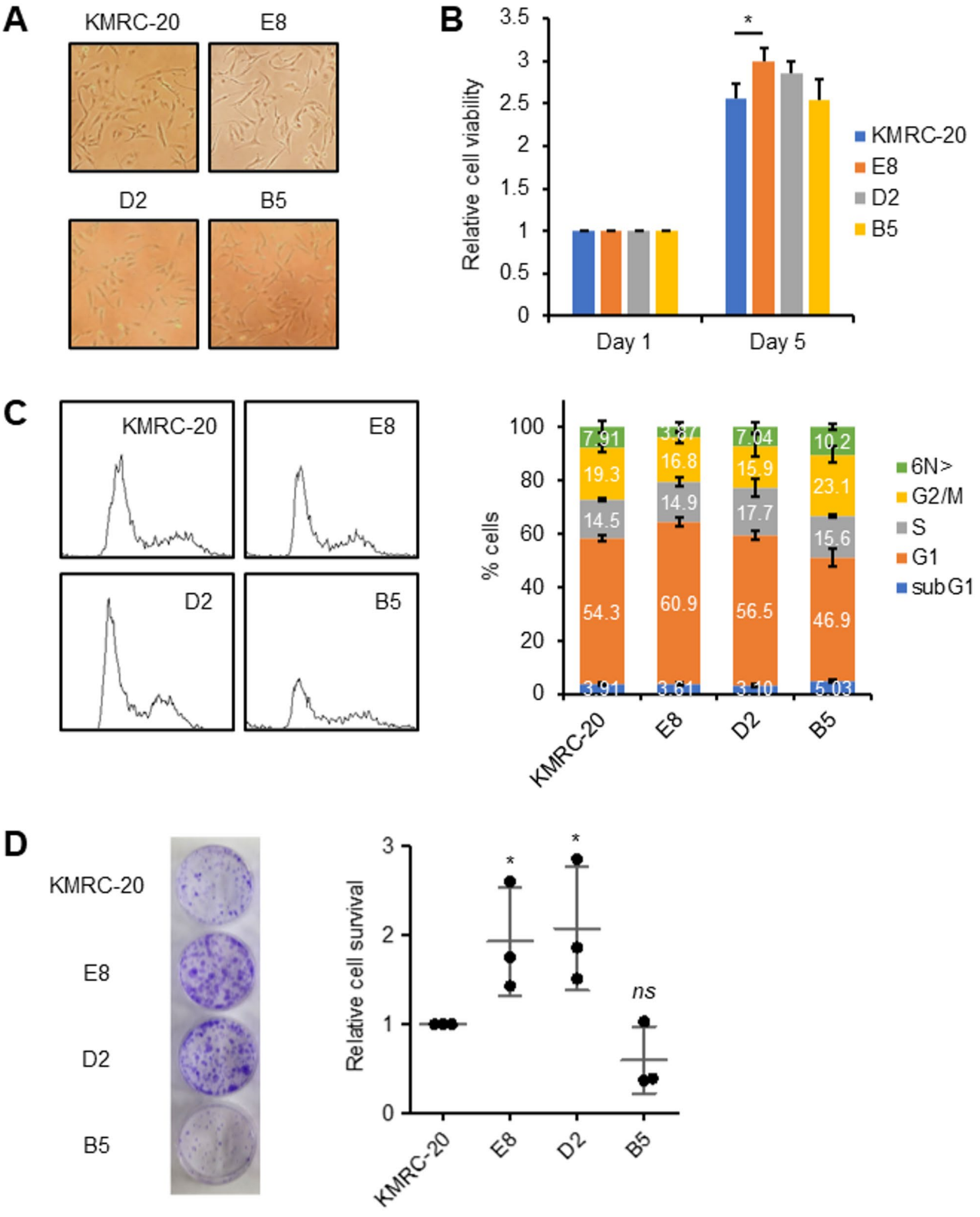


Fig. 2 General characteristics of revertant KMRC-20 cells: morphology, cell cycle profile, and proliferation (**A**) Representative microscopic images of parental and revertant KMRC-20 cells showing overall morphology. (**B**) MTS assay results assessing short-term cell viability. Relative viability was normalized to day 1 values (set to 1). Experiments were performed in triplicate. $n = 3$; mean ± s.d. (**C**) Cell cycle profiles determined by flow cytometry. Representative histograms are shown, with quantification of sub-G1 (apoptotic), G1, S, G2/M, and polyploid populations presented to the right. $n = 3$; mean ± s.d. (**D**) Colony formation assay results evaluating long-term clonogenic potential. Representative colony images are shown with quantification of colony numbers to the right. Experiments were performed in triplicate. $n = 3$; mean ± s.d

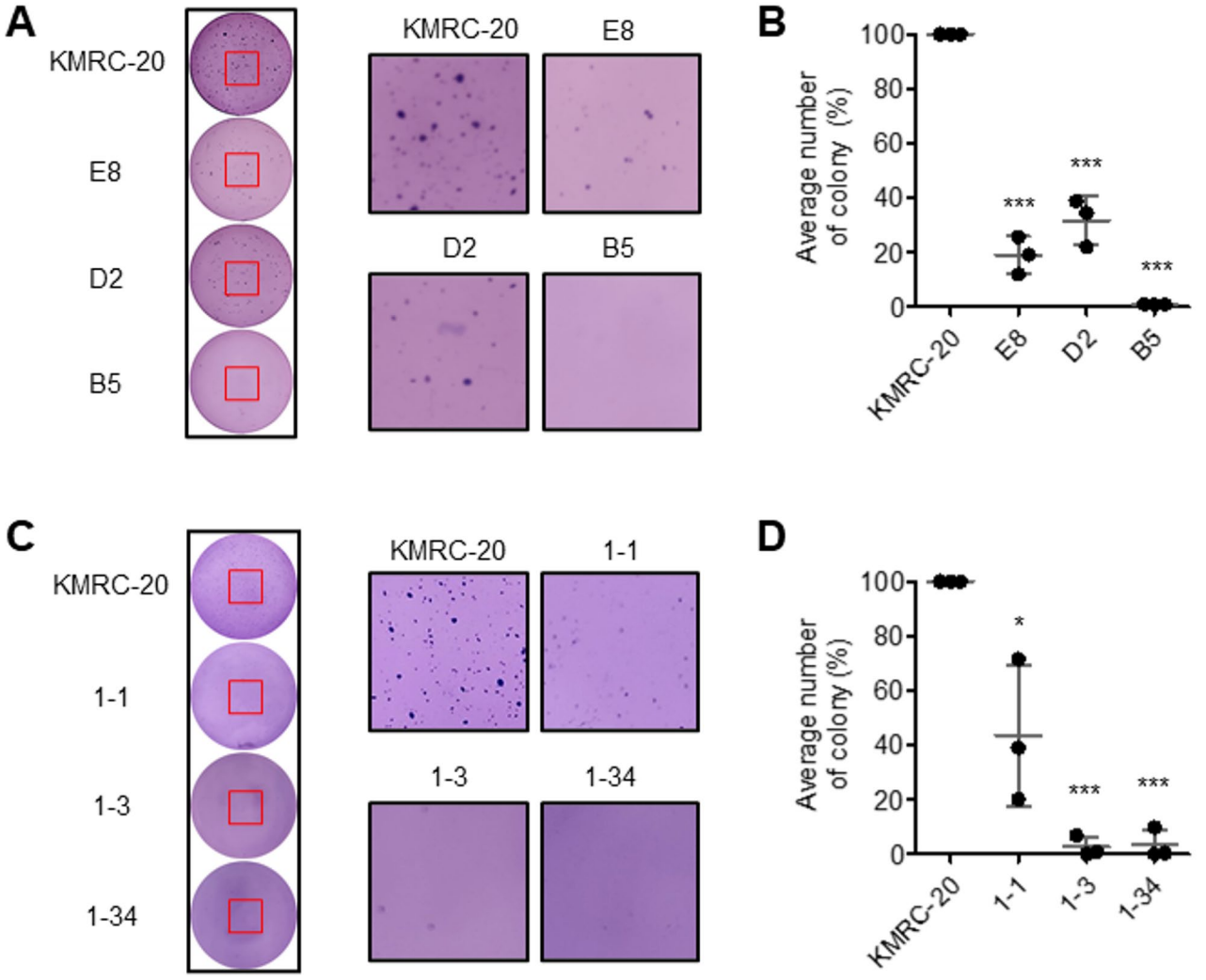


Fig. 3 BAP1 reactivation restores anchorage-dependent growth in KMRC-20 cells (**A**) Soft agar assay results assessing anchorage-dependent growth of parental and revertant KMRC-20 clones (E8, D2, and B5). Representative images of colonies are shown, with magnified views of boxed regions presented to the right. (**B**) Quantification of colony numbers from (A), normalized to parental cells (set to 100). Experiments were performed in triplicate. $n = 3$; mean ± s.d. (**C**, **D**) Soft agar assay results for additional revertant clones (1–1, 1–3, and 1–34) shown as in (**A**) and (**B**)

We assessed whether the levels of these proteins were altered under anchorage loss. After 48 h of culture in ULA conditions, N-cadherin levels were significantly reduced in all three revertant clones compared to parental KMRC-20 cells, while remaining stable under adherent conditions, with only a modest reduction in clone 1–3. In contrast, vimentin expression remained unchanged across both conditions (Fig. 5A). β-catenin levels in the revertant cells also decreased under ULA conditions (Fig. 5B).

To confirm that these effects were specifically linked to restoration of BAP1 function via Glu31, we generated an additional control cell line, designated 1-1-G31, by introducing a single base substitution in the 1–1 revertant clone to convert the Glu31 codon (GAG) to GGG, encoding glycine. This mutation rendered BAP1 catalytically inactive in vitro and within cells. Sequencing confirmed the precise edit with no mutations at the top three predicted off-target sites (Fig. 5C and Fig. S5). In 1-1-G31 cells, both N-cadherin and β-catenin levels were restored to levels comparable to parental KMRC-20 cells, while remaining significantly downregulated in the original 1–1 revertant cells (Fig. 5D). Importantly, apoptosis under ULA conditions—as assessed by PARP1 cleavage—was reduced in 1-1-G31 cells relative to the 1–1 revertant, supporting the loss of BAP1 function (Fig. 5D). These results confirm that the downregulation of N-cadherin and β-catenin in revertant cells is specific to the reactivation of BAP1 catalytic activity.

Together, these findings demonstrate that N-cadherin and β-catenin are selectively downregulated in BAP1-revertant cells under anchorage-independent conditions,

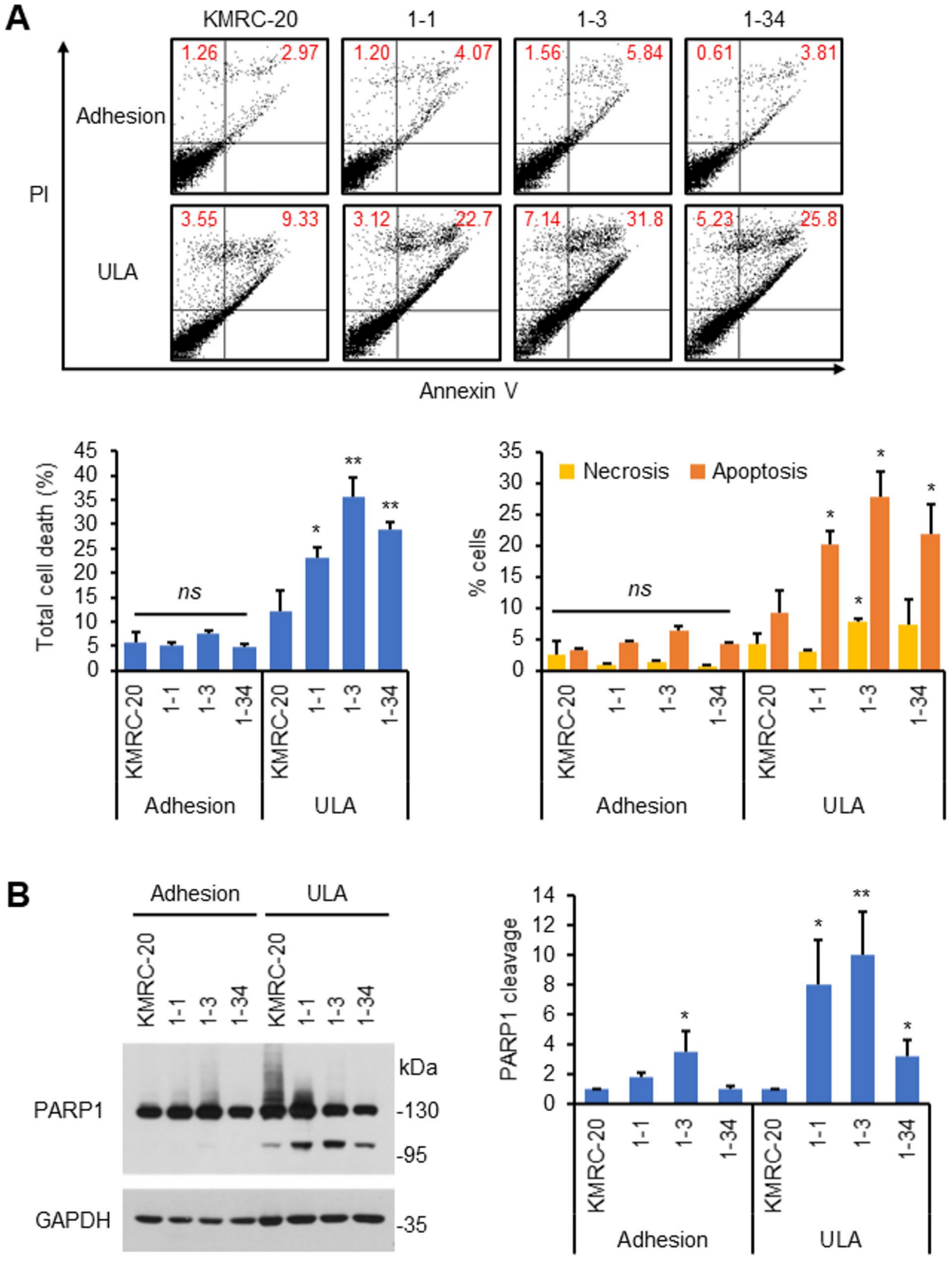


Fig. 4 (See legend on next page.)

(See figure on previous page.)

Fig. 4 BAP1 reactivation induces apoptosis in KMRC-20 cells under anchorage-free conditions (**A**) Apoptosis assay results showing increased apoptosis in revertant KMRC-20 cells under non-adherent conditions. Parental and revertant KMRC-20 cells were cultured either on standard adherent dishes or on ultra-low attachment (ULA) plates for 24 h, followed by Annexin V/PI staining and flow cytometric analysis. (Top) Representative dot plots are shown, with percentages of necrotic cells (upper left quadrant) and apoptotic cells (upper right + lower right quadrants) indicated. (Bottom) Quantification of total cell death (necrosis + apoptosis) (left) and separate quantification of apoptotic and necrotic populations (right) are presented. $n = 3$; mean ± s.d. (**B**) Confirmation of increased apoptosis in revertant KMRC-20 cells under anchorage-free conditions by immunoblot analysis of PARP1 cleavage. Representative immunoblots are shown, with quantification of relative PARP1 cleavage presented to the right, normalized to the parental value in each culture condition. $n = 3$; mean ± s.d

while vimentin expression remains unaffected. This pattern suggests that BAP1 may support anchorage-dependent growth not through global reversal of EMT, but rather by selectively influencing pro-survival signaling associated with cell adhesion and Wnt/β-catenin pathways.

N-cadherin and β-catenin expression is regulated post-transcriptionally in revertant KMRC-20 cells

To determine the mechanism underlying the downregulation of N-cadherin and β-catenin proteins in the revertant cells under anchorage loss, we investigated whether these changes occur at the transcriptional or post-transcriptional level. Parental KMRC-20 cells and the three revertant clones were cultured under either adherent or ULA conditions, and total RNA was extracted for quantitative RT-PCR analysis of N-cadherin and β-catenin mRNA levels. As shown in Fig. 6, mRNA levels of both genes remained largely unchanged across all conditions in the revertant clones compared to the parental cells. Notably, no significant differences were observed between adherent and ULA culture conditions. These results suggest that the observed downregulation of N-cadherin and β-catenin proteins upon anchorage loss is not due to decreased gene transcription but is instead mediated by post-transcriptional mechanisms, potentially involving regulation of protein stability or degradation.

Transcriptomic analysis reveals broad gene expression changes upon BAP1 reactivation in KMRC-20 cells

To investigate genome-wide transcriptional changes associated with BAP1 reactivation, we performed RNA-sequencing analysis comparing the parental KMRC-20 cells with two revertant clones, 1–1 and 1–34. Hierarchical clustering of global gene expression profiles revealed that the revertant clones clustered distinctly from the parental cells, indicating widespread transcriptional reprogramming following restoration of BAP1 activity. Differential expression analysis identified a substantial number of genes altered by at least two-fold between the parental and revertant groups (Fig. S6A).

Gene ontology (GO) enrichment analysis of differentially expressed genes (DEGs) revealed that the transcriptional changes in the revertant cells spanned diverse biological processes, including Wnt signaling, epithelial cell proliferation, cell adhesion, and apoptosis (Fig. 7 and Fig. S6B). These findings align with the observed phenotypic differences between parental and revertant cells, particularly with respect to anchorage-dependent growth. Notably, N-cadherin and β-catenin were not among the DEGs identified in either clone, consistent with our RT-PCR data indicating that their regulation occurs post-transcriptionally. These transcriptomic data suggest that, in addition to post-transcriptional regulation of key adhesion-related proteins, BAP1 restoration in KMRC-20 cells induces broader changes in gene expression. Whether these changes arise directly from BAP1 reactivation or indirectly as a downstream consequence of altered adhesion-associated signaling remains unclear. Nonetheless, such transcriptional responses may collectively reinforce anchorage-dependent growth and contribute to the suppression of tumorigenic behavior under non-adherent conditions.

Discussion

In this study, we examined the functional consequences of the Glu31 mutation in BAP1—a recurrent missense alteration observed in ccRCC—which impairs both its enzymatic activity and protein stability. Using CRISPR-Cas9–mediated adenine base editing, we precisely reverted the Glu31Lys mutation to the wild-type glutamate in the KMRC-20 cell line, which harbors this as its sole BAP1 coding mutation. This strategy enabled the generation of stable, isogenic revertant clones and allowed us to investigate BAP1's tumor suppressor functions under physiological expression levels, thereby avoiding artifacts commonly associated with gene overexpression systems.

We demonstrated that correction of the Glu31 mutation restores BAP1's DUB activity, stabilizes the protein, and recovers its previously reported role in DNA repair. Notably, BAP1 reactivation re-established anchorage-dependent growth in KMRC-20 cells—a defining feature of non-transformed epithelial cells. This phenotypic change was accompanied by increased apoptosis under non-adherent culture conditions, indicating a restored sensitivity to anoikis [31, 32]. These findings uncover a previously unrecognized role for BAP1 in suppressing anchorage-independent survival—a hallmark of tumorigenic transformation—highlighting the therapeutic

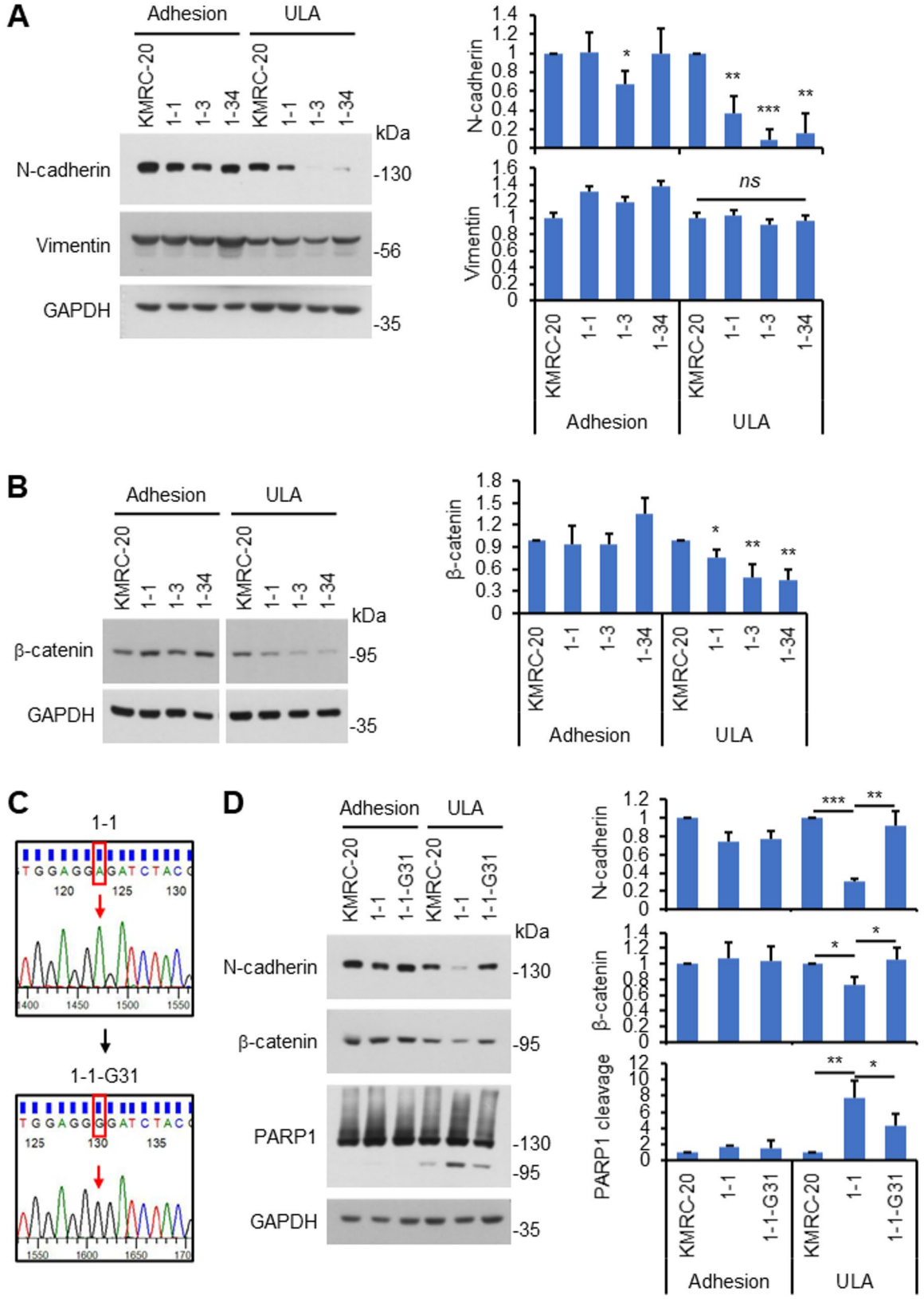


Fig. 5 (See legend on next page.)

(See figure on previous page.)

Fig. 5 BAP1 reactivation downregulates N-cadherin and b-catenin in revertant KMRC-20 cells under anchorage-free conditions (**A**) Immunoblot analysis showing decreased N-cadherin levels, but not vimentin, in revertant KMRC-20 cells under non-adherent conditions. Parental and revertant cells were cultured on standard adherent dishes or ULA plates for 48 h and subjected to immunoblotting. Representative blots are shown, with quantification of protein band intensity presented to the right, normalized to the parental value in each culture condition. $n = 3$; mean ± s.d. (**B**) Immunoblot analysis showing decreased β-catenin levels in revertant KMRC-20 cells under non-adherent conditions. Parental and revertant cells were cultured as in (A) for 48 h, followed by immunoblotting. Representative blots are shown, with quantification presented to the right as in (A). $n = 3$; mean ± s.d. The adhesion and ULA panels were derived from the same original gel. (**C**) Sequencing of genomic DNA from the 1-1-G31 clone demonstrating reversion of the corrected wild-type glutamate codon (GAG) back to the Glu31Gly mutation (GGG). (**D**) Immunoblot analysis showing loss of BAP1 reactivation-associated phenotypes in the 1-1-G31 clone following BAP1 re-inactivation. The 1-1-G31 clone exhibits restored N-cadherin and β-catenin levels, along with reduced PARP1 cleavage compared to its parental 1–1 clone. Cells were cultured as in (A) for 48 h and analyzed by immunoblotting. Representative blots are shown, with quantification presented to the right as in (A)

potential of precise gene editing to restore BAP1 tumor suppressor function in ccRCC.

ccRCC is the most prevalent subtype of kidney cancer and is defined by frequent deletions on chromosome 3p, where several key tumor suppressor genes—*VHL*, *PBRM1*, *SETD2*, and *BAP1*—are located. Among these, *VHL* is most commonly inactivated through biallelic mutations, resulting in dysregulation of the cellular oxygen-sensing pathway and establishment of a persistent pseudo-hypoxic state that promotes tumorigenesis. However, *VHL* loss alone is insufficient to drive full transformation; co-inactivation of one of the other 3p tumor suppressors is frequently observed and thought to be essential for malignant progression [39, 40]. BAP1, in particular, plays multifaceted roles in tumor suppression, notably in maintaining genomic stability through its involvement in DNA repair and promoting apoptosis in response to genotoxic stress [15].

Our study reveals an additional tumor-suppressive function of BAP1 that has not been fully appreciated in the context of ccRCC: the suppression of anchorage-independent survival. By restoring BAP1 function via precise correction of a cancer-associated point mutation, we demonstrate that BAP1 prevents survival of cells under non-adherent conditions, thereby reinstating anoikis—a critical barrier to metastasis that is often bypassed in cancer. These findings extend the current understanding of BAP1's role in ccRCC, highlighting its capacity to restrain multiple malignant features, including resistance to cell death, genomic instability, and potentially metastatic dissemination. This expanded view of BAP1 function reinforces its significance as a therapeutic target and a pivotal node in the tumor suppressor network disrupted in ccRCC.

Although our data suggest that BAP1 reactivation post-transcriptionally downregulates N-cadherin and β-catenin under anchorage-free conditions, the mechanisms underlying this regulation remain unresolved, and the absence of identified direct BAP1 targets represent a key limitation of our study. Given BAP1's established role as a deubiquitinase that stabilizes specific substrates, the observed reduction in N-cadherin and β-catenin is likely an indirect effect. One possibility is that BAP1 stabilizes E3 ubiquitin ligases that, in turn, promote ubiquitination and proteasomal degradation of these proteins, thereby facilitating their turnover in response to loss of adhesion. Several E3 ubiquitin ligases known or implicated to target N-cadherin and β-catenin—including Hakai (CBLL1) [41], members of the MARCH family [42], SCF^{b-TRCP} [43, 44], and TRIM33 [45]—represent potential candidates. BAP1 might also contribute by destabilizing protective protein complexes or displacing binding partners, rendering N-cadherin and β-catenin more susceptible to degradation [15]. In addition to these indirect pathways, direct mechanisms cannot be excluded. For example, BAP1 could modulate the ubiquitination status of N-cadherin and β-catenin by removing non-degradative K63-linked ubiquitin chains while leaving K48-linked ubiquitin signals intact, thereby sensitizing these proteins to proteasomal degradation under anchorage-free conditions [46]. Alternatively, BAP1 may influence post-transcriptional regulators, such as RNA-binding proteins or microRNAs, that control the translation of N-cadherin and β-catenin transcripts. Thus, our working model consider both indirect and direct possibilities by which BAP1 might suppress anchorage-independent survival. Additional studies will be needed to delineate these pathways and to more clearly define the BAP1-dependent signaling network governing adhesion-dependent apoptosis.

In conclusion, our study suggests that a single point mutation in BAP1—commonly found in ccRCC—may compromise its tumor suppressor function by affecting protein stability, enzymatic activity, and anchorage-dependent cell death. By employing base editing to precisely correct this mutation in isogenic cell lines, we restored BAP1 function and uncovered its role in suppressing anchorage-independent survival through post-transcriptional downregulation of N-cadherin and β-catenin. To our knowledge, this represents the first application of base editing to investigate the physiological impact of a recurrent BAP1 mutation in cancer. Overall, these findings provide insight into mechanisms of BAP1-driven tumorigenesis and point to the potential of precise genome editing approaches for restoring tumor suppressor activity.

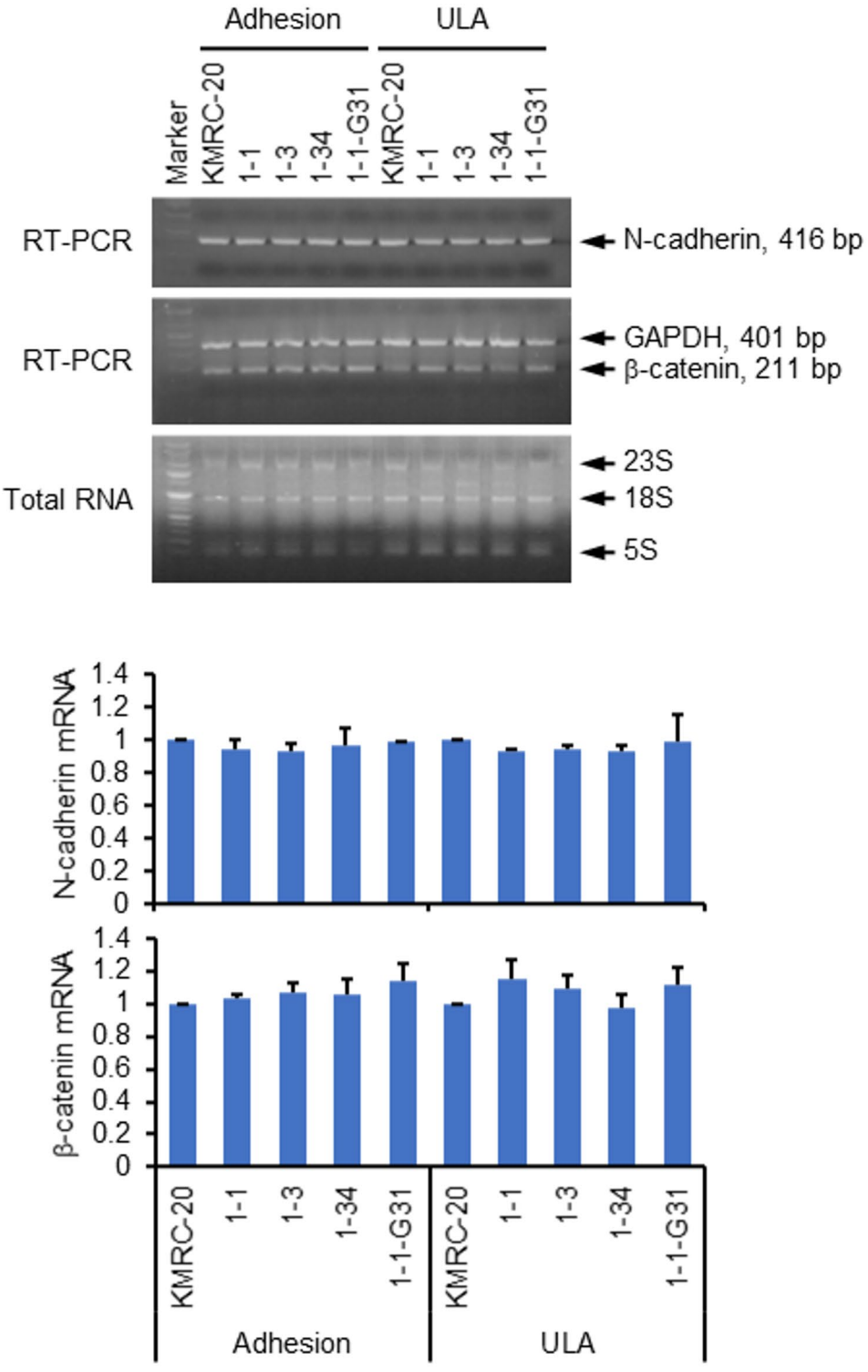


Fig. 6 N-cadherin and β-catenin downregulation in revertant KMRC-20 cells under anchorage-free conditions occur via post-transcriptional mechanisms RT-PCR analysis showing unchanged mRNA levels of N-cadherin and β-catenin upon BAP1 reactivation or re-inactivation in KMRC-20 cells, regardless of adhesion status. Parental and revertant KMRC-20 cells, as well as the 1-1-G31 clone, were cultured on standard adherent dishes or ULA plates for 24 h, followed by total RNA isolation and RT-PCR analysis. Sizes of RT-PCR products for N-cadherin and β-catenin, with GAPDH as an internal control, are indicated. Representative agarose gels are shown, with quantification presented to the right, normalized to parental values in each condition. Marker, 1 kb DNA ladder

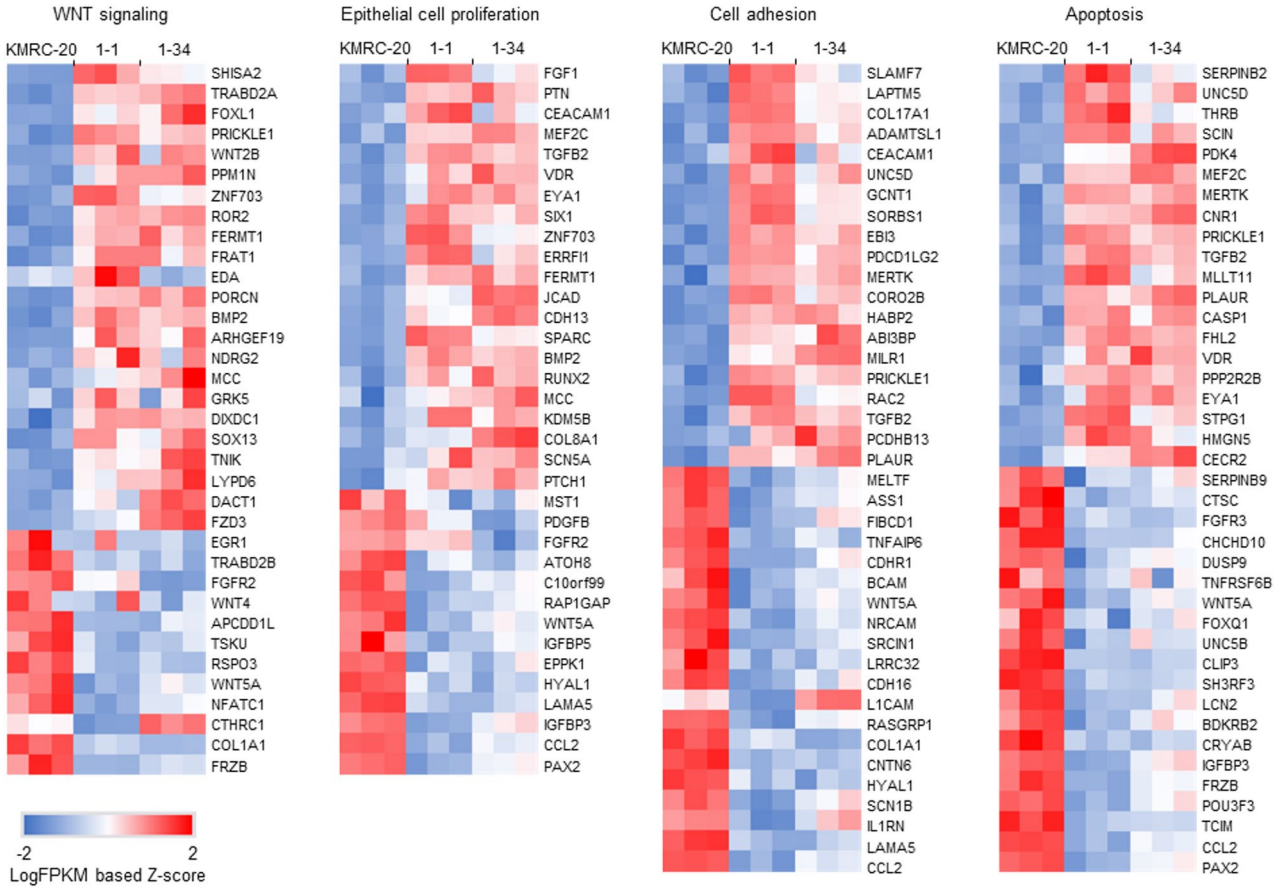


Fig. 7 Transcriptomic analysis reveals broad gene expression changes upon BAP1 reactivation in KMRC-20 cells Heat map of differentially expressed genes (fold change ≥ 2) associated with Wnt signaling, epithelial cell proliferation, cell adhesion, and apoptosis pathway. Total RNA was isolated from three independent cultures each of parental KMRC-20 cells, clone 1–1, and clone 1–34, and subjected to RNA-sequencing analysis. Gene expression values were normalized using TPM (Transcripts Per Million) and log2-transformed prior to analysis. Differentially expressed genes were identified using exactTest with Benjamini–Hochberg correction (raw p-value < 0.05). Hierarchical clustering was performed using complete linkage and Euclidean distance metrics to visualize expression patterns. Gene symbols are shown to the right of the corresponding heat map rows

Materials & methods

Cells and antibodies

The KMRC-20 cell line (JCRB1071) was obtained from the JCRB Cell Bank (Japan). Parental and revertant KMRC-20 cells were cultured in Dulbecco's Modified Eagle's Medium (DMEM) supplemented with 10% fetal bovine serum (FBS; Hyclone), 100 U/mL penicillin, and 100 μg/mL streptomycin. For revertant KMRC-20 clones generated by lentiviral transduction (clones E8, D2, and B5), puromycin was added at a final concentration of 4 μg/mL two to three times per week to maintain selection. HEK293T, HCT116, and HeLa cells were obtained from the American Type Culture Collection (ATCC, Manassas, VA) and maintained in their respective recommended media. All cell lines were cultured at 37 °C in a humidified incubator with 5% CO_2. The cell lines were authenticated with DNA fingerprinting using short tandem repeat markers every 50 passages and were tested for the absence of Mycoplasma contamination using the e-Myco VALiD Mycoplasma PCR Detection Kit (Intron Biotechnology).

The following primary antibodies were used in this study: anti-BAP1 (mouse IgG, sc-28383; rabbit IgG, sc-28236), anti-PARP1 (sc-8007), and anti-β-actin (sc-8432) from Santa Cruz Biotechnology; anti-γ-H2AX (06–636) and anti-H2A (07–146) from Millipore; anti-GAPDH (LF-PA0212) from AbFrontier; anti-cyclobutane pyrimidine dimers (CPD; CAC-NM-DND-001) from Cosmo Bio; and anti-H2A (12349), anti-β-catenin (9582), anti-N-cadherin (13116), anti-vimentin (5741), and anti-Cas9 (19526) from Cell Signaling Technology.

Generation of revertant KMRC-20 cell lines by base editing

To correct the *BAP1* Glu31Lys mutation (AAG to GAG) in KMRC-20 cells, we selected the VRQR variant of ABE7.10max as a suitable adenine base editor [30]. This editor, which recognizes an NGAG protospacer adjacent motif (PAM) and efficiently deaminates the adenine within AAG codons, was originally engineered in

a lentiviral vector containing a puromycin resistance marker to target the *LMNA* gene in Hutchinson-Gilford Progeria Syndrome (HGPS) (Addgene plasmid #154429). To redirect its specificity toward the Glu31 mutation in *BAP1*, the vector was modified by replacing the original gRNA with a BAP1-targeting gRNA (5′-gga gaa gat cta cga cct tc-3′) through two rounds of site-directed mutagenesis. The oligonucleotides used for gRNA replacement were as follows: first round, 5′-cga aac acc ggg aga aga tcc tgg gct ccg-3′ (forward) and 5′-cgg agc cca. gga tct tct ccc ggt gtt tcg-3′(reverse); second round, 5′-cac cgg gag aag atc tac gac ctt cgt ttt aga gc-3′ (forward) and 5′-gct cta aaa cga agg tcg tag atc ttc tcc cgg tg-3′ (reverse). The resulting construct, ABE7.10max-VRQR-BAP1, was verified by sequencing to confirm successful gRNA replacement.

To generate the revertant clones E8, D2, and B5, the ABE7.10max-VRQR-BAP1 construct was transfected into HEK293T cells using FuGENE HD transfection reagent (Promega, E2311). After 48 h, lentivirus-containing supernatant was harvested, filtered through a 0.45 μm syringe filter, and used to infect KMRC-20 cells. Infected cells were selected with puromycin (4 μg/mL) and then subjected to limited serial dilution in 96-well plates to isolate individual clones. Genomic DNA was extracted using Exgene™ Cell SV (GeneAll), and the region encompassing the target site was PCR-amplified and sequenced to confirm base editing. The three top-predicted off-target sites were similarly amplified and sequenced to assess off-target editing.

To generate an independent set of revertant clones (1–1, 1–3, and 1–34), the ABE7.10max-VRQR-BAP1 plasmid was directly transfected into KMRC-20 cells using Lipofectamine LTX with PLUS reagent (Invitrogen), followed by puromycin selection and clonal isolation as described above. Clone 1-1-G31 was generated from clone 1–1 by a subsequent round of bystander editing using the same plasmid and transfection protocol. All clones were verified by sequencing of the edited locus and screened for off-target mutations by sequencing the same three predicted off-target sites.

Ub-AMC assay using BAP1 immune complexes

For analysis of BAP1 deubiquitinase activity, a total of 1×10^6 KMRC-20 cells were harvested and lysed in NP-40 lysis buffer containing 50 mM Tris-Cl (pH 8.0), 150 mM NaCl, 1% NP-40, and 5 mM EDTA for 30 min on ice. Lysates were sonicated for 20 min and centrifuged at 16,000 × g for 20 min at 4 °C to remove debris. The resulting supernatants were pre-cleared with protein G agarose beads (Millipore) overnight at 4 °C. Following centrifugation, the pre-cleared lysates were divided into two equal portions and incubated overnight at 4 °C with either anti-BAP1 antibody or isotype-matched control IgG, followed by protein G agarose to capture immune complexes. Beads were collected by centrifugation, washed thoroughly with NP-40 lysis buffer, and then with DUB buffer (20 mM HEPES, pH 7.5, 150 mM NaCl, 0.1 mg/mL BSA, and 1 mM DTT). The washed beads were resuspended in DUB buffer and divided into two aliquots: one for immunoblotting and the other for Ub-AMC enzymatic assay. For the assay, ubiquitin-7-amido-4-methylcoumarin (Ub-AMC) substrate (Boston Biochem) was added to the immune complexes, and reactions were performed in black 96-well plates at room temperature. Fluorescence signals were measured every 30 s using a SpectraMax i3X microplate reader (Molecular Devices) at an excitation wavelength of 350 nm and an emission wavelength of 450 nm (NFEC-2019-10–258101, Ewha Fluorescence Core Imaging Center).

Cell viability assay

For cell viability assessment, 1,000 cells were seeded per well in 96-well plates and cultured under standard conditions for seven days. Cell proliferation was quantified using the CellTiter AQueous One Solution Cell Proliferation Assay (MTS assay; Promega, G3580) according to the manufacturer's instructions. Briefly, CellTiter AQueous reagent was added directly to the wells and incubated for 1 h at 37 °C. Absorbance was measured at 490 nm using a microplate reader. For colony formation assays to assess clonogenic ability, 1,000 cells were seeded into 35-mm culture dishes and maintained for 14 days. At the end of the incubation period, colonies were fixed and stained with crystal violet, and colony formation was evaluated.

Anchorage-independent growth assays

Soft agar assays were performed to assess anchorage-independent growth. A base layer of 0.6% low-melting-point agarose in PBS was poured into 35-mm dishes and allowed to solidify. Cells (2×10^4 per dish) were suspended in 0.4% low-melting-point agarose in PBS and layered on top of the base agar. The plates were incubated for five weeks at 37 °C in a humidified 5% CO_2 incubator. At the end of the incubation, colonies were stained with 0.001% crystal violet in 20% ethanol and counted using ImageJ software.

Cell cycle analysis

1×10^5 cells were harvested and fixed in ice-cold 70% ethanol overnight. The fixed cells were then washed twice with PBS and resuspended in PBS containing propidium iodide (PI) prior to flow cytometric analysis using a FACSCalibur system (BD Biosciences).

Apoptosis assay

For apoptosis detection, Annexin V/PI double staining was performed using the FITC Annexin V Apoptosis Detection Kit I (556547, BD Biosciences) according to the manufacturer's instructions. Briefly, 2×10^5 cells were washed twice with PBS and resuspended in 1 mL of binding buffer. A 100 µL aliquot of the cell suspension was mixed with 5 µL of FITC-conjugated Annexin V and 5 µL of PI (Invitrogen), gently vortexed, and incubated at room temperature for 20 min in the dark. Samples were then analyzed by flow cytometry using an LSRFortessa (BD Biosciences) (NFEC-2019-10–258102, Ewha Fluorescence Core Imaging Center).

RT-PCR

Total RNA was extracted from cells using TRIzol reagent (Favogen) according to the manufacturer's instructions. Three micrograms of total RNA were reverse-transcribed into cDNA using HelixCript thermo reverse transcriptase (Nanohelix, RT50K) and random hexamer primers (Promega, C1181). The resulting cDNA was used as a template for PCR amplification, and the PCR products were resolved on 2% agarose gels. The following primers were used: GAPDH (35 cycles): 5'-ccc ttc att gac ctc aac tac-3' (forward) 5'-cca aag ttg tca tgg atg acc-3' (reverse); N-cadherin, 5′-cac tgc tca gga ccc aga t-3′ (forward), 5′-taa gcc gag tga tgg tcc-3′; β-catenin, 5'-acg gag gaa ggt ctg agg ag-3' (forward), 5'-agc cgc ttt tct gtc tgg tt-3' (reverse).

RNA-sequencing analysis

RNA-seq analysis was performed as previously described. A total of 1 µg of RNA extracted from cells was used to construct cDNA libraries using the TruSeq Standard mRNA Sample Prep Kit (Illumina, 20020595). The libraries were quantified with the KAPA Library Quantification Kit for Illumina platforms (KAPA BIOSYSTEMS, KK4854), following the PCR Quantification protocol guide, and qualified using the TapeStation D1000 ScreenTape system (Agilent Technologies). Paired-end sequencing was performed on the Illumina NovaSeq platform. Cleaned reads were aligned to the Homo sapiens reference genome (GRCh38) using HISAT v2.1.0, which implements both HISAT and Bowtie2 algorithms. The genome sequence and gene annotations were obtained from the NCBI Genome Assembly and RefSeq databases. After alignment, transcript assembly and quantification were conducted using StringTie v2.1.3b. Gene- and transcript-level expression values were calculated as raw read counts, FPKM (Fragments Per Kilobase of transcript per Million mapped reads), and TPM (Transcripts Per Million). Differential expression analysis was performed using the exactTest, and fold change and p-values were extracted accordingly. All p-values were adjusted for multiple testing using the Benjamini-Hochberg procedure to control the false discovery rate (FDR). Genes with $|\text{fold change}| \geq 2$ and raw p-value < 0.05 were considered significantly differentially expressed. Hierarchical clustering of these genes was conducted using complete linkage and Euclidean distance to assess expression pattern similarities. All data analysis and visualization of differentially expressed genes were performed using R version 3.6.0 (www.r-project.org).

CPD assay

The cyclobutane pyrimidine dimer (CPD) assay was performed as previously described. Briefly, 1×10^5 cells were seeded onto poly-L-lysine-coated coverslips and allowed to adhere before being irradiated with UV-C light at a dose of 10 J/m². Following irradiation, cells were incubated for the indicated time periods and then fixed with methanol for 10 min at room temperature. DNA denaturation was achieved by incubating cells with 2 M HCl for 30 min. After washing, cells were blocked in 3% bovine serum albumin (BSA) in PBS for 1 h. The cells were incubated with an anti-CPD monoclonal antibody (Cosmo Bio, CAC-NM-DND-001) for 1 h at room temperature, followed by a secondary incubation with Alexa Fluor 568-conjugated goat anti-mouse IgG (Thermo Fisher Scientific) for 30 min. After washing with PBS containing 0.1% Tween-20 (PBS-T), the stained cells were mounted onto glass slides using VECTASHIELD Mounting Medium with DAPI (Vector Laboratories). Confocal images were acquired using a Carl Zeiss LSM 880 confocal laser scanning microscope (NFEC-2016-05–209580, Ewha Fluorescence Core Imaging Center). Image processing and quantification of CPD staining intensity were performed using ZEN 2.3 software (Carl Zeiss).

Immunoblot analysis

Whole-cell lysates were prepared using RIPA buffer containing 50 mM Tris-Cl (pH 8.0), 150 mM NaCl, 0.5% sodium deoxycholate, 0.1% SDS, 1% NP-40, 0.5 mM PMSF, 10 mM NaF, and a protease inhibitor cocktail. Protein concentrations were quantified using the BCA Protein Assay Kit (Pierce) according to the manufacturer's instructions. Equal amounts of protein were mixed with SDS sample loading buffer, boiled for 5 min, and subjected to SDS-PAGE. Proteins were transferred to membranes and immunoblotting was performed following standard protocols using appropriate primary and HRP-conjugated secondary antibodies. Detection was carried out using chemiluminescence reagents. For the detection of Ub-H2A and H2A, histone proteins were extracted and analyzed by immunoblotting using anti-H2A antibody as previously described.

Statistical analysis

Statistical significance was evaluated using the unpaired Student's *t*-test, performed with Microsoft Excel and GraphPad Prism 5 software. Data are presented as mean ± standard deviation (SD), and *p*-values less than 0.05 were considered statistically significant. Statistical significance is indicated as follows: $p < 0.05$ (*), $p < 0.01$ (**), $p < 0.001$ (***), and $p > 0.05$ (*ns*, not significant).

Supplementary Information

The online version contains supplementary material available at https://doi.org/10.1186/s12935-025-04082-5.

Supplementary Material 1

Author contributions

D.L., B.L., and J.L. performed the experiments and generated the data. D.L. and J.K. wrote the manuscript. J.K. conceived and supervised the entire project.

Funding

This work was supported by grants 2023R1A2C3005307 (JK) and 2022R1I1A1A01073047 (DL) from the National Research Foundation of Korea.

Data availability

No datasets were generated or analysed during the current study.

Declarations

Ethics approval and consnent to participate

Our studies did not include human participants, human tissues or other animal subjects.

Competing interests

The authors declare no competing interests.

Received: 22 August 2025 / Accepted: 12 November 2025
Published online: 25 November 2025

References

1. Jensen DE, Proctor M, Marquis ST, Gardner HP, Ha SI, Chodosh LA, Ishov AM, Tommerup N, Vissing H, Sekido Y, et al. BAP1: a novel ubiquitin hydrolase which binds to the BRCA1 RING finger and enhances BRCA1-mediated cell growth suppression. Oncogene. 1998;16(9):1097–112.
2. Carbone M, Yang H, Pass HI, Krausz T, Testa JR, Gaudino G. BAP1 and cancer. Nat Rev Cancer. 2013;13(3):153–9.
3. Misaghi S, Ottosen S, Izrael-Tomasevic A, Arnott D, Lamkanfi M, Lee J, Liu J, O'Rourke K, Dixit VM, Wilson AC. Association of C-terminal ubiquitin hydrolase BRCA1-associated protein 1 with cell cycle regulator host cell factor 1. Mol Cell Biol. 2009;29(8):2181–92.
4. Machida YJ, Machida Y, Vashisht AA, Wohlschlegel JA, Dutta A. The deubiquitinating enzyme BAP1 regulates cell growth via interaction with HCF-1. J Biol Chem. 2009;284(49):34179–88.
5. Lee HS, Lee SA, Hur SK, Seo JW, Kwon J. Stabilization and targeting of INO80 to replication forks by BAP1 during normal DNA synthesis. Nat Commun. 2014;5:5128.
6. Lee HS, Seo HR, Lee SA, Choi S, Kang D, Kwon J. BAP1 promotes stalled fork restart and cell survival via INO80 in response to replication stress. Biochem J. 2019;476(20):3053–66.
7. Yu H, Pak H, Hammond-Martel I, Ghram M, Rodrigue A, Daou S, et al. Tumor suppressor and deubiquitinase BAP1 promotes DNA double-strand break repair. Proc Natl Acad Sci U S A. 2014;111(1):285–90.
8. Szczepanski AP, Wang L. Emerging multifaceted roles of BAP1 complexes in biological processes. Cell Death Discov. 2021;7(1):20.
9. Seo HR, Jeong D, Lee S, Lee HS, Lee SA, Kang SW, et al. CHIP and BAP1 act in concert to regulate INO80 ubiquitination and stability for DNA replication. Molecules Cells. 2021;44(2):101–15.
10. Daou S, Hammond-Martel I, Mashtalir N, Barbour H, Gagnon J, Iannantuono NV, Nkwe NS, Motorina A, Pak H, Yu H, et al. The BAP1/ASXL2 histone H2A deubiquitinase complex regulates cell proliferation and is disrupted in cancer. J Biol Chem. 2015;290(48):28643–63.
11. Zhang Y, Shi J, Liu X, Feng L, Gong Z, Koppula P, Sirohi K, Li X, Wei Y, Lee H, et al. BAP1 links metabolic regulation of ferroptosis to tumour suppression. Nat Cell Biol. 2018;20(10):1181–92.
12. Kuznetsov JN, Aguero TH, Owens DA, Kurtenbach S, Field MG, Durante MA, et al. BAP1 regulates epigenetic switch from pluripotency to differentiation in developmental lineages giving rise to BAP1-mutant cancers. Sci Adv. 2019;5(9):eaax1738.
13. Dey A, Seshasayee D, Noubade R, French DM, Liu J, Chaurushiya MS, Kirkpatrick DS, Pham VC, Lill JR, Bakalarski CE, et al. Loss of the tumor suppressor BAP1 causes myeloid transformation. Science. 2012;337(6101):1541–6.
14. Bononi A, Giorgi C, Patergnani S, Larson D, Verbruggen K, Tanji M, et al. BAP1 regulates IP3R3-mediated Ca(2+) flux to mitochondria suppressing cell transformation. Nature. 2017;546(7659):549–53.
15. Masclef L, Ahmed O, Estavoyer B, Larrivee B, Labrecque N, Nijnik A, Affar EB. Roles and mechanisms of BAP1 deubiquitinase in tumor suppression. Cell Death Differ. 2021;28(2):606–25.
16. Qin J, Zhou Z, Chen W, Wang C, Zhang H, Ge G, Shao M, You D, Fan Z, Xia H, et al. BAP1 promotes breast cancer cell proliferation and metastasis by deubiquitinating KLF5. Nat Commun. 2015;6:8471.
17. Kang M, Park SG, Lee SA, Kim S, Lee D, Shirbhate ME, Youn SY, Kim KM, Cha SS, Kwon J. Targeting BAP1 with small compound inhibitor for colon cancer treatment. Sci Rep. 2023;13(1):2264.
18. Bononi A, Yang H, Giorgi C, Patergnani S, Pellegrini L, Su M, Xie G, Signorato V, Pastorino S, Morris P, et al. Germline BAP1 mutations induce a Warburg effect. Cell Death Differ. 2017;24(10):1694–704.
19. Mashtalir N, Daou S, Barbour H, Sen NN, Gagnon J, Hammond-Martel I, Dar HH, Therrien M. Affar El B: autodeubiquitination protects the tumor suppressor BAP1 from cytoplasmic sequestration mediated by the atypical ubiquitin ligase UBE2O. Mol Cell. 2014;54(3):392–406.
20. Scheuermann JC, de Ayala Alonso AG, Oktaba K, Ly-Hartig N, McGinty RK, Fraterman S, et al. Histone H2A deubiquitinase activity of the Polycomb repressive complex PR-DUB. Nature. 2010;465(7295):243–7.
21. Harbour JW, Onken MD, Roberson ED, Duan S, Cao L, Worley LA, Council ML, Matatall KA, Helms C, Bowcock AM. Frequent mutation of BAP1 in metastasizing uveal melanomas. Science. 2010;330(6009):1410–3.
22. Testa JR, Cheung M, Pei J, Below JE, Tan Y, Sementino E, Cox NJ, Dogan AU, Pass HI, Trusa S, et al. Germline BAP1 mutations predispose to malignant mesothelioma. Nat Genet. 2011;43(10):1022–5.
23. Pena-Llopis S, Vega-Rubin-de-Celis S, Liao A, Leng N, Pavia-Jimenez A, Wang S, et al. BAP1 loss defines a new class of renal cell carcinoma. Nat Genet. 2012;44(7):751–9.
24. Carbone M, Harbour JW, Brugarolas J, Bononi A, Pagano I, Dey A, Krausz T, Pass HI, Yang H, Gaudino G. Biological mechanisms and clinical significance of BAP1 mutations in human cancer. Cancer Discov. 2020;10(8):1103–20.
25. Carbone M, Adusumilli PS, Alexander HR Jr., Baas P, Bardelli F, Bononi A, et al. Mesothelioma: scientific clues for prevention, diagnosis, and therapy. CA Cancer J Clin. 2019;69(5):402–29.
26. Kwon J, Lee D, Lee SA. BAP1 as a guardian of genome stability: implications in human cancer. Exp Mol Med. 2023;55(4):745–54.
27. Lee SA, Lee D, Kang M, Kim S, Kwon SJ, Lee HS, et al. BAP1 promotes the repair of UV-induced DNA damage via PARP1-mediated recruitment to damage sites and control of activity and stability. Cell Death Differ. 2022. https://doi.org/10.1038/s41418-022-01024-w.
28. Pickar-Oliver A, Gersbach CA. The next generation of CRISPR-Cas technologies and applications. Nat Rev Mol Cell Biol. 2019;20(8):490–507.
29. Anzalone AV, Koblan LW, Liu DR. Genome editing with CRISPR-Cas nucleases, base editors, transposases and prime editors. Nat Biotechnol. 2020;38(7):824–44.
30. Koblan LW, Erdos MR, Wilson C, Cabral WA, Levy JM, Xiong ZM, Tavarez UL, Davison LM, Gete YG, Mao X, et al. In vivo base editing rescues Hutchinson-Gilford Progeria syndrome in mice. Nature. 2021;589(7843):608–14.
31. Paoli P, Giannoni E, Chiarugi P. Anoikis molecular pathways and its role in cancer progression. Biochim Biophys Acta. 2013;1833(12):3481–98.
32. Gerstberger S, Jiang Q, Ganesh K. Metastasis. Cell. 2023;186(8):1564–79.

33. Suskiewicz MJ, Prokhorova E, Rack JGM, Ahel I. ADP-ribosylation from molecular mechanisms to therapeutic implications. Cell. 2023;186(21):4475–95.
34. van Roy F. Beyond E-cadherin: roles of other cadherin superfamily members in cancer. Nat Rev Cancer. 2014;14(2):121–34.
35. Mrozik KM, Blaschuk OW, Cheong CM, Zannettino ACW, Vandyke K. N-cadherin in cancer metastasis, its emerging role in haematological malignancies and potential as a therapeutic target in cancer. BMC Cancer. 2018;18(1):939.
36. Pecina-Slaus N. Wnt signal transduction pathway and apoptosis: a review. Cancer Cell Int. 2010;10:22.
37. Polakis P. Wnt signaling and cancer. Genes Dev. 2000;14(15):1837–51.
38. Kalluri R, Weinberg RA. The basics of epithelial-mesenchymal transition. J Clin Invest. 2009;119(6):1420–8.
39. Cotta BH, Choueiri TK, Cieslik M, Ghatalia P, Mehra R, Morgan TM, et al. Current landscape of genomic biomarkers in clear cell renal cell carcinoma. Eur Urol. 2023;84(2):166–75.
40. Webster BR, Gopal N, Ball MW. Tumorigenesis mechanisms found in hereditary renal cell carcinoma: a review. Genes (Basel). 2022. https://doi.org/10.3390/genes13112122.
41. Escuder-Rodriguez JJ, Rodriguez-Alonso A, Jove L, Quiroga M, Alfonsin G, Figueroa A. Beyond destruction: emerging roles of the E3 ubiquitin ligase Hakai. Cell Mol Biol Lett. 2025;30(1):9.
42. Seo T, Lowery AM, Xu H, Giang W, Troyanovsky SM, Vincent PA, et al. MARCH family E3 ubiquitin ligases selectively target and degrade cadherin family proteins. PLoS ONE. 2024;19(5):e0290485.
43. Winston JT, Strack P, Beer-Romero P, Chu CY, Elledge SJ, Harper JW. The SCF-beta-TRCP-ubiquitin ligase complex associates specifically with phosphorylated destruction motifs in IkappaBalpha and beta-catenin and stimulates IkappaBalpha ubiquitination in vitro. Genes Dev. 1999;13(3):270–83.
44. Liu C, Kato Y, Zhang Z, Do VM, Yankner BA, He X. Beta-Trcp couples beta-catenin phosphorylation-degradation and regulates xenopus axis formation. Proc Natl Acad Sci U S A. 1999;96(11):6273–8.
45. Xue J, Chen Y, Wu Y, Wang Z, Zhou A, Zhang S, Lin K, Aldape K, Majumder S, Lu Z, et al. Tumour suppressor TRIM33 targets nuclear beta-catenin degradation. Nat Commun. 2015;6:6156.
46. Estavoyer B, Messmer C, Echbicheb M, Rudd CE, Milot E, Affar EB. Mechanisms orchestrating the enzymatic activity and cellular functions of deubiquitinases. J Biol Chem. 2022;298(8):102198.

Publisher's note

Springer Nature remains neutral with regard to jurisdictional claims in published maps and institutional affiliations.